Materials Advances

ROYAL SOCIETY OF CHEMISTRY

PAPER

View Article Online
View Journal | View Issue

Check for updates

Cite this: *Mater. Adv.*, 2025, **6**, 9806

# Synthesis of iron-based metal–organic frameworks and carbon derivatives *via* unconventional synthetic methods and waste precursors with potential for gas storage

Keaoleboga Mosupi,[ab] Nqobile T. Mthembu,[a] Mike Masukume,[b] Nicholas M. Musyoka*[c] and Henrietta W. Langmi*[a]

Received 1st September 2025,
Accepted 26th October 2025

DOI: 10.1039/d5ma00994d

rsc.li/materials-advances

Metal–organic frameworks (MOFs) have remarkable characteristics including high porosity as well as large internal surface areas. However, these materials have found very limited use industrially due to their high cost of production. The use of waste materials and industrial by-products to generate cheaper and environmentally friendly precursors could potentially open doors for industrial production of MOFs. Two types of Fe-based MOFs (Fe-MIL-53 and Fe-MIL-88B) were prepared using acid mine drainage (AMD) waters as a metal precursor source and waste polyethylene terephthalate-derived terephthalic acid (PET-BDC) as a linker *via* microwave-assisted and sonochemical-assisted synthesis procedures. Additionally, a carbonization strategy was utilized to enhance the porosity and surface area of these MOF materials. Upon carbonization, surface areas were drastically improved to above 600 $m^2\ g^{-1}$ for both MIL-53 and MIL-88B prepared using the two unconventional methods. The obtained carbons also exhibited reasonable gas uptake capacities, with MIL-53 derived carbons having a higher hydrogen capacity of 1.32 wt% (at 77 K and 1 bar) and a carbon dioxide capacity of 2.09 mmol $g^{-1}$ (at 298 K and 1 bar). The gas uptake capacities of MIL-88B derived carbons were found to be relatively low.

Open Access Article. Published on 12 november 2025. Downloaded on 11-05-2026 16:36:12.
This article is licensed under a Creative Commons Attribution 3.0 Unported Licence.

## 1. Introduction

More than 20 years after metal–organic frameworks (MOFs) were discovered, the progress towards industrialization has been slow.[1] There are a few industrial players such as BASF, NuMat Technologies, MOF Technologies and novoMOF who have up-scaled the synthesis of MOFs.[2] Wide-scale MOF industrialization is mainly impeded by the lack of affordable and sustainable synthetic methods. The conventional solvothermal synthesis process also faces challenges such as long synthetic time and requirements for high pressure and temperatures, in addition to the use of harsh and toxic solvents.[3] Synthetic methods including microwave-assisted, sonochemical-assisted, flow chemistry, electrochemistry, mechanochemical and dry heating synthesis provide alternative and viable routes for industrialization. In addition, MOF precursors could also be derived from unconventional sources. For example, organic ligands can be obtained from waste polyethylene terephthalate (PET), biomass and industrial by-product or waste.[4–6] To demonstrate the viability of waste-derived MOFs, Wang and Wang prepared Fe-MIL-88B, Fe-MIL-53, Co-MOFs and Ni-MOFs using a PET-derived organic linker and the MOFs were evaluated for synergistic flame retardancy.[7] Gonçalves *et al.* synthesized 3d transition metal MOFs (Fe, Co, Ni, Cu and Zn) employing an organic linker derived from PET and the prepared materials were tested for adsorption of methylene blue, methyl orange, Nile blue and malachite green.[8] Several other studies have employed PET derived terephthalic acid for synthesis of various MOFs for a range of applications.[9–11] On the other hand, metal precursors have previously been obtained from unconventional sources, such as coal fly ash, mined raw minerals, domestic waste materials and even from industrial by-products.[12] Precursors derived from waste materials or low-cost raw materials provide an ecofriendly and cost-effective pathway to MOF industrialization.[13]

Importantly, the holistic combination of unconventional synthetic methods with waste-derived precursors not only contributes to the development of advanced MOF materials but also addresses pressing environmental issues related to industrial waste disposal and resource recycling. This innovative approach paves the way for more sustainable and inexpensive

[a] *Department of Chemistry, University of Pretoria, Private Bag X20, Hatfield, 0028, South Africa. E-mail: Henrietta.Langmi@up.ac.za*
[b] *Centre for Nanostructures and Advanced Materials (CeNAM), Chemicals cluster, Council for Scientific and Industrial Research (CSIR), Meiring Naude Road, Brummeria, Pretoria, 0001, South Africa*
[c] *Nottingham Ningbo China Beacons of Excellence Research and Innovation Institute, University of Nottingham Ningbo China, Ningbo, 315100, P. R. China. E-mail: nicholas.musyoka@nottingham.edu.cn*


© 2025 The Author(s). Published by the Royal Society of Chemistry

Open Access Article. Published on 12 november 2025. Downloaded on 11-05-2026 16:36:12.
This article is licensed under a Creative Commons Attribution 3.0 Unported Licence.

production of iron-based MOFs (Fe-MOFs), which can have a transformative impact on various industrial and environmental applications. In this case, this study employs microwave-assisted and sonochemical-assisted synthesis methods for the preparation of flexible Fe-MIL-53 and Fe-MIL-88B MOFs. The organic linker, terephthalic acid ($H_2BDC$), was derived from waste-PET bottles, whereas the iron precursor was derived from acid mine drainage (AMD), a by-product of mining activities.

The rationale for choosing MIL-53 and MIL-88B was their known 'breathing effect' since their one-dimensional pores may contract or dilate depending on applied heat, pressure or guest molecules.[14–16] Several studies have shown that Fe-MIL-53 tends to maintain the narrow-collapsed pores even upon heating or when subjected to $N_2$ adsorption.[17–19] Permanent porosity and improved surface area can be achieved in these materials through direct carbonization. Furthermore, carbonization of MOFs is often known to introduce varying pore structures, which are beneficial for various applications. For example, a previous study on carbonization of MIL-88B at elevated pyrolysis temperatures led to a significant improvement in the specific surface area, soaring from 170 to 265 $m^2\ g^{-1}$, indicating enhanced porosity and structural evolution of the carbon framework.[20]

This study focused on the preparation of iron-based MIL-53 and MIL-88B and their carbon derivatives using AMD-derived iron and PET-derived BDC *via* microwave-assisted and sonochemical-assisted synthesis methods. The prepared carbons were then evaluated for hydrogen ($H_2$) and carbon dioxide ($CO_2$) storage applications.

## 2. Experimental

### 2.1. Conversion of wastes into reagents

Iron was extracted from AMD water by oxidative precipitation as outlined previously.[21] Briefly, 30 mL of 30% hydrogen peroxide ($H_2O_2$) was introduced to 1000 mL of AMD water under continuous agitation at room temperature for 1.5 h. Then, a pH of 3.5 was obtained by a dropwise addition of 4 M sodium hydroxide (NaOH) solution. This was followed by agitation of the solution for an additional 15 min. The resulting iron sediment was isolated by vacuum filtration, extensively washed with deionized water (1000 mL) to remove any impurities, and subsequently dried in a conventional oven at 80 °C for 12 h. The extract was confirmed to be iron hydroxide.

To extract $H_2BDC$ from waste, a published procedure was followed.[4] In this case, 12.5 g of PET flakes was combined with 12.5 mL of ethylene glycol (EG) and 300 mL of deionized water in a 500 mL autoclave. The temperature of the autoclave was increased to 210 °C and maintained for 8 h to promote depolymerization. Upon reaching ambient conditions, the reaction solution was centrifuged to isolate the sediment, which was subsequently washed twice using ethanol and oven-dried at 100 °C for 24 h. The product was confirmed to be $H_2BDC$ in accordance with the study by Dyosiba *et al.*[4] The recovered $H_2BDC$, derived from PET, served as the organic ligand in the subsequent MOF synthesis.

### 2.2. Metal–organic framework synthesis

**2.2.1. Microwave synthesis.** To synthesize Fe-MIL-88B, 0.6655 g of AMD-derived iron precursor was added to 5 mL of hydrochloric acid (HCl) and heated at 70 °C until dissolution. Separately, the organic ligand solution was formulated by dissolving 0.4462 g of PET-derived $H_2BDC$ in a solution of dimethylformamide (DMF, 50 mL) and acetic acid (5 mL) using ultrasonic agitation. Following transfer to a four-necked round-bottom flask, the reaction mixture was heated up to 80 °C in a microwave reactor operated at 500 W for 4 h. Upon reaching ambient conditions, the sediment was recovered by centrifugation, rinsed three times with 50 mL of fresh DMF to remove unreacted precursors, and then subjected to three successive ethanol washes (3 × 50 mL) to exchange solvents. The sample was vacuum-dried at 60 °C overnight and designated as Micro-MIL-88B.

Fe-MIL-53 was prepared following a similar synthetic method to that described for Fe-MIL-88B without the addition of acetic acid and using a shorter time of 2 h. The resulting sample was designated as Micro-MIL-53.

**2.2.2. Sonochemical synthesis.** For the preparation of Fe-MIL-88B, the metal and organic ligand solution was prepared in the same manner as in the microwave synthesis. The solution was introduced into a four-necked round bottom flask, which was transferred to a sonochemical reactor and subjected to continuous ultrasonication using a probe operating at 80% of its maximum frequency for 4 h. The washing and drying steps were similar to those employed in the microwave method. The sample was designated as Sono-MIL-88B.

Fe-MIL-53 was synthesized following an analogous method to that described for Fe-MIL-88B but without the addition of acetic acid and using a shorter reaction time of 2 h and 60% of its maximum frequency. The sample was designated as Sono-MIL-53.

### 2.3. MDC synthesis

Each of the synthesized MOFs was individually used to prepare carbon materials. In this procedure, 0.5 g of MOF was loaded into a crucible and carbonized at 600 °C (10 °C $min^{-1}$) for 2 h under a $N_2$ atmosphere in a tube furnace. The iron–carbon composite obtained was washed with 70 mL of HCl (32%) at 70 °C for 4 h. This was followed by vacuum filtration and rinsing repetitively with deionized water. The obtained carbon material was oven-dried at 100 °C for 12 h. The obtained carbons were designated as Sono-MDC-53 or Sono-MDC-88B (derived from Sono-MIL-53 or Sono-MIL-88B, respectively) and Micro-MDC-53 or Micro-MDC-88B (derived from Micro-MIL-53 or Micro-MIL-88B, respectively).

### 2.4. Characterization

A Malvern Panalytical Aeris diffractometer using Fe-filtered Co-Kα radiation was used to collect X-ray diffraction (XRD) data in the range of $2\theta$ = 5–60° at a scanning rate of 0.2° $s^{-1}$. A JASCO FT/IR-4X Fourier transform infrared (FTIR) spectrometer was employed to confirm the functional groups of the prepared

Open Access Article. Published on 12 november 2025. Downloaded on 11-05-2026 16:36:12.
This article is licensed under a Creative Commons Attribution 3.0 Unported Licence.

MOFs. The spectra were obtained between 4000 and 650 $cm^{-1}$ at a resolution of 16 $cm^{-1}$, and background elimination was conducted. Morphological features of MOFs were examined using a JEOL-JSM 7500F scanning electron microscope (SEM). Textural properties were obtained using a Quantachrome autosorb iQ instrument with analysis performed using $N_2$ gas at 77 K. The non-local density functional theory (NLDFT) model was used to derive pore size distribution and pore volumes of the synthesized materials. A Micromeritics 3Flex instrument was used to record $H_2$ and $CO_2$ adsorption isotherms at 77 K and 298 K, respectively, and up to a pressure of 1 bar. Prior to gas analysis, samples were degassed at 150 °C for 12 h. A TA Instruments Q500 model thermogravimetric analyzer was utilized to determine the moisture content and decomposition behavior of the prepared samples. For this analysis, samples were placed on alumina crucibles heated to 900 °C at a heating rate of 10 °C $min^{-1}$. Thermogravimetric analysis for both MOFs and carbons was performed under a flow of atmospheric air.

## 3. Results and discussion

### 3.1. Powder X-ray diffraction

XRD patterns presented in Fig. 1a and b validate the synthesis of the individual Fe-MIL-53 and Fe-MIL-88B from both sonochemical and microwave-assisted methods. The observed diffraction peaks closely matched those described in previous studies, validating the successful formation of the target crystalline phase.[22,23] Prominent diffraction peaks of Fe-MIL-53 are observed at 9.3, 12.4, 16.5, 17.3, 18.7, 21.8, 25.9 and 28.2° corresponding to (110), (200), (011), (111), (220), (121), (400) and (321) planes. Synthesized Sono-MIL-88B displayed prominent diffraction peaks at 9.39 and 10.3° with additional reflections at 12.58, 18.86, 19.34 and 22°, which are consistent with the reflections for the trinuclear d-block metal containing MOFs (Fig. 1b). The identified peaks are associated with the (002), (101), (102), (103), (200), and (201) crystallographic planes. The pattern for the synthesized Micro-MIL-88B exhibited an additional sharp peak at 7.8°, which is ascribed to the high crystallinity of the sample.[24–26] The sharp high intensity diffraction peaks of the Micro-MIL-88B indicate the higher crystallinity of this sample compared to that of Sono-MIL-88B. This high crystallinity arises from the more uniform and controlled crystal growth afforded by the microwave-assisted method. The pattern for Sono-MIL-88B displayed comparatively broad low intensity peaks. The low crystallinity of Sono-MIL-88B and the absence of the peak at 7.8° (100) might be due to the presence of defects and/or disorders. Broad and low intensity peaks of MIL-88B have been previously reported.[27] The XRD results have shown that AMD-derived iron and PET-derived $H_2BDC$ were successfully converted into Fe-MIL-53 and Fe-MIL-88B *via* sonochemical and microwave-assisted methods.

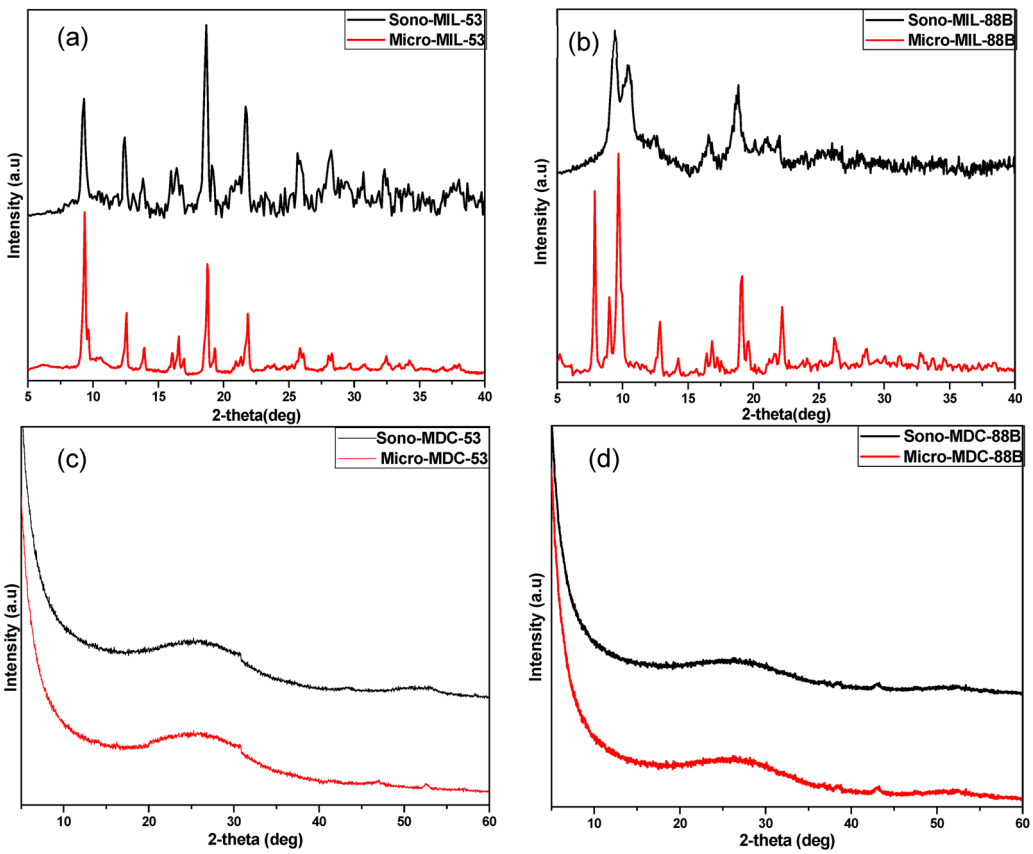


Fig. 1 X-ray diffraction patterns of (a) Fe-MIL-53, (b) Fe-MIL-88B, (c) MDC-53 and (d) MDC-88B.


© 2025 The Author(s). Published by the Royal Society of Chemistry

Open Access Article. Published on 12 november 2025. Downloaded on 11-05-2026 16:36:12.
This article is licensed under a Creative Commons Attribution 3.0 Unported Licence.

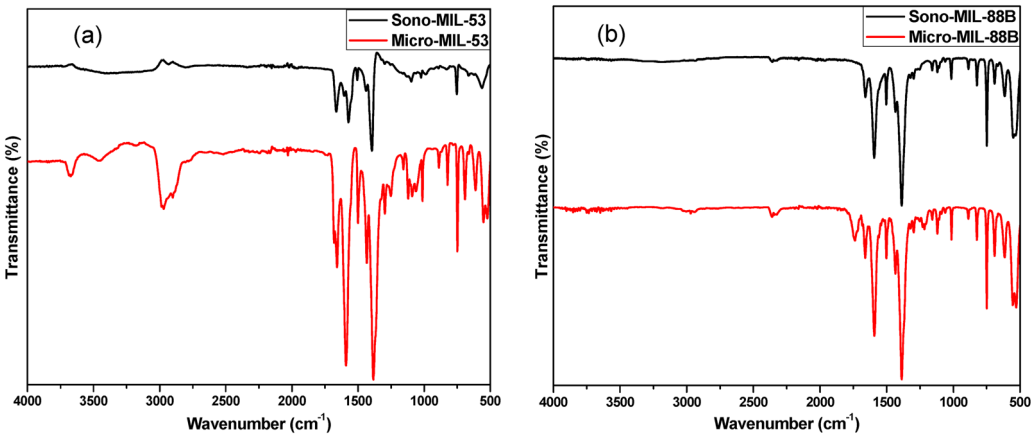


Fig. 2 FTIR spectra of (a) Fe-MIL-53 and (b) Fe-MIL-88B.

After successfully synthesizing these MOFs, they were subsequently converted into carbon materials. The direct carbonization under inert conditions at a high temperature resulted in a broad diffraction peak between 20 and 30° for all the MDCs, which is assigned to the (002) plane (Fig. 1c and d). The carbon material may have formed *via* two possible processes, *i.e.* the carboxylic ligand transforming into carbon and/or an *in situ* redox reaction in which carbon reduced $Fe^{3+}$, which led to cleavage of the Fe–O coordination bond, thus resulting in reduced Fe (0) species. The reduced species leads to a local reductive environment, thus promoting the formation of turbostratic carbon structures. This phenomenon has been observed by other researchers.[28–30] The lack of additional peaks in the XRD patterns for all the MDCs signifies the successful acid wash of the synthesized carbon materials.

### 3.2. Fourier transform infrared spectroscopy

Molecular architecture and functional moieties of the synthesized MOFs were examined using FTIR spectroscopy, as displayed in Fig. 2. The Micro-MIL-53 sample displayed a peak at 3670 $cm^{-1}$, which signifies the presence of the –OH group as a result of trapped $H_2O$ molecules. The peak at 2972 $cm^{-1}$ represents the $C_{sp3}$–H stretches. The residual materials in the pores of the MOF can be removed using the combination of solvent exchange and high temperature (605 K) activation, as shown by Wang *et al.*[31] Ahnfeldt *et al.* and Boutin *et al.* also showed that solvent exchange and high temperature activation are beneficial for the removal of trapped molecules in MOF pores.[32,33] The Sono-MIL-53 sample does not display bands at 3670 and 2972 $cm^{-1}$ due to the absence of $H_2O$. Vibrational bands common to both Fe-MIL-53 samples can be observed, for instance, the bands at 1661 $cm^{-1}$ (C–O, free organic linker/DMF), 1592 and 1386 $cm^{-1}$ (asymmetric and symmetric C═O), 1064 $cm^{-1}$ (C–O–Fe), 751 $cm^{-1}$ (out-of-plane C–H) and 554 $cm^{-1}$ (Fe–O) as shown in Fig. 2a.[28,34] Fig. 2b shows the FTIR spectra of Fe-MIL-88B. Bands at 550 $cm^{-1}$ (Fe–O stretching), 748 $cm^{-1}$ (C–H bending), 1398 and 1505 $cm^{-1}$ (symmetric and asymmetric C═O stretching), 1659 $cm^{-1}$ (C–O stretching, free organic linker/DMF), and 1096 $cm^{-1}$ (C–O–Fe stretching) verify the successful formation of Fe-MIL-88B.[35–37]

### 3.3. Scanning electron microscopy

SEM was employed to elucidate the morphology of both Fe-MIL-53 and Fe-MIL-88B as well as their carbon derivates. The obtained hexagonal bipyramidal morphology of the MOFs

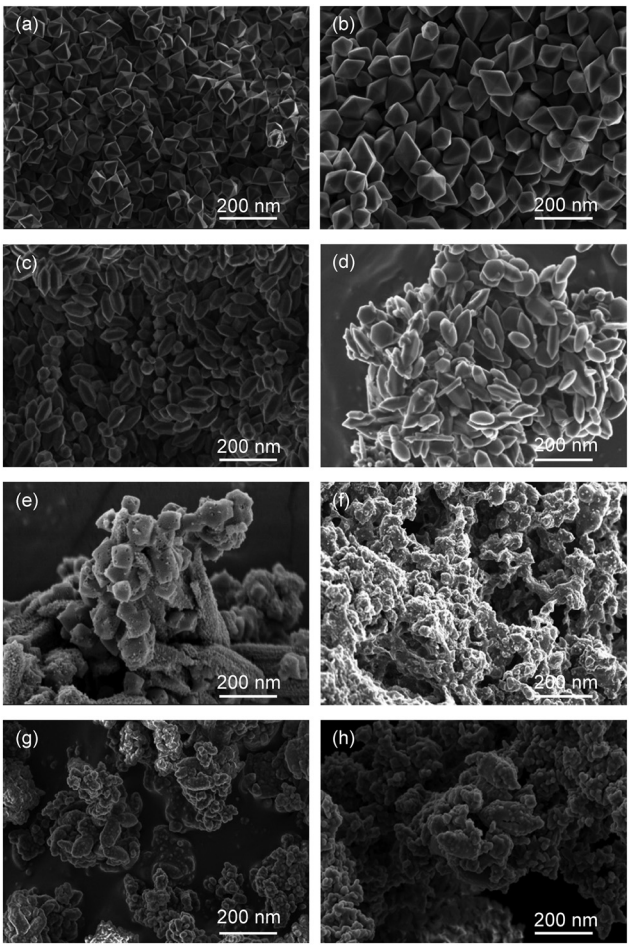


Fig. 3 SEM images of (a) Micro-MIL-53, (b) Sono-MIL-53, (c) Micro-MIL-88B, (d) Sono-MIL-88B, (e) Micro-MDC-53, (f) Sono-MDC-53, (g) Micro-MDC-88B and (h) Sono-MDC-88B.

Open Access Article. Published on 12 november 2025. Downloaded on 11-05-2026 16:36:12.
This article is licensed under a Creative Commons Attribution 3.0 Unported Licence.

coincides with previously reported findings (Fig. 3a–d).[38–41] The resulting carbonized materials (Fig. 3e–h) consist of relatively amorphous, heterogeneous and defect-rich particles. The morphology of the parent MOF materials is preserved to some extent, while the MDCs are mainly made of interconnected small carbon particles.

### 3.4. Thermogravimetric analysis

Thermal decomposition of the prepared MOFs was analyzed using TGA. The TGA plots for all MOF samples are shown in Fig. 4a and b, which exhibit a multi-step weight loss. Moisture and/or DMF on the surface and within pores of the MOF tend to evaporate at temperatures below 200 °C, which explains the first weight loss for both cases. The second decomposition step at 360 °C could be associated with the possibility of unreacted organic ligand/DMF within the pores of the material (as corroborated by the FTIR spectrum (band at 1659 $cm^{-1}$)). The subsequent mass loss at 400 °C is attributed to decomposition of the coordinated organic ligand for MIL-88B and MIL-53 samples, respectively. The remaining materials are the thermodynamically stable iron clusters. The reported profiles are consistent with previous reports.[42–44]

The thermal robustness of the derived carbons was studied under atmospheric air conditions across a temperature of 25–900 °C, as shown in Fig. 4c and d. The initial mass loss at temperatures below 100 °C is attributed to the loss of physisorbed moisture. The carbons are thermally stable until 430 °C, after which complete combustion of the material occurs. The complete loss of weight indicates the successful acid wash, where all iron metal species were successfully removed from the carbons.

### 3.5. Raman analysis

The extent of potential graphitization, structural defects and amorphous nature of the MDCs were evaluated by employing Raman spectroscopy, as shown in Fig. 5. Correspondingly, all spectra displayed both the D-band (~1355 $cm^{-1}$) and the G-band (~1600 $cm^{-1}$), which are associated with the graphitic material.[45] Th D-band signifies the presence of defects or disorders derived from the vibrations of the $sp^3$ bonds. In contrast, the G-band arises from the in-plane vibrational stretching of the $sp^2$-hybridized carbon–carbon bonds typically found in graphitic structures. The D-to-G band intensity ratio can serve as the indicator of the graphitic configuration, with the higher value indicating the amorphous nature and high number of defects.[46] The presence of the $sp^3$ bonds might be due to the removal of the iron clusters by acid wash. The intensity ratio (1.29–1.67, Table 1) is associated with the turbostratic nature of the derived carbons.[47] The lack of graphitization might be ascribed to the low carbonization temperature.

### 3.6. Textural properties

Fig. 6a displays the $N_2$ adsorption–desorption isotherms of Fe-MIL-53 at 77 K. The isotherms exhibit a combination of

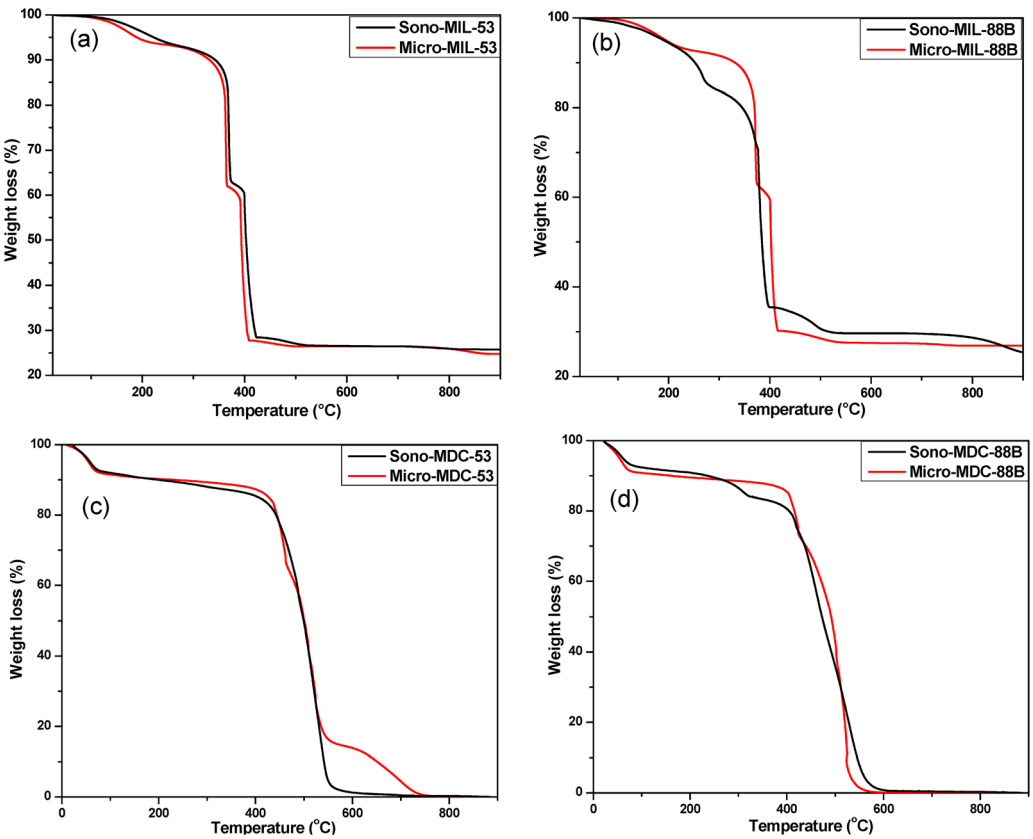


Fig. 4 TGA profiles of (a) Fe-MIL-53, (b) Fe-MIL-88B, (c) MDC-53 and (d) MDC-88B samples.


© 2025 The Author(s). Published by the Royal Society of Chemistry

Open Access Article. Published on 12 november 2025. Downloaded on 11-05-2026 16:36:12.
This article is licensed under a Creative Commons Attribution 3.0 Unported Licence.

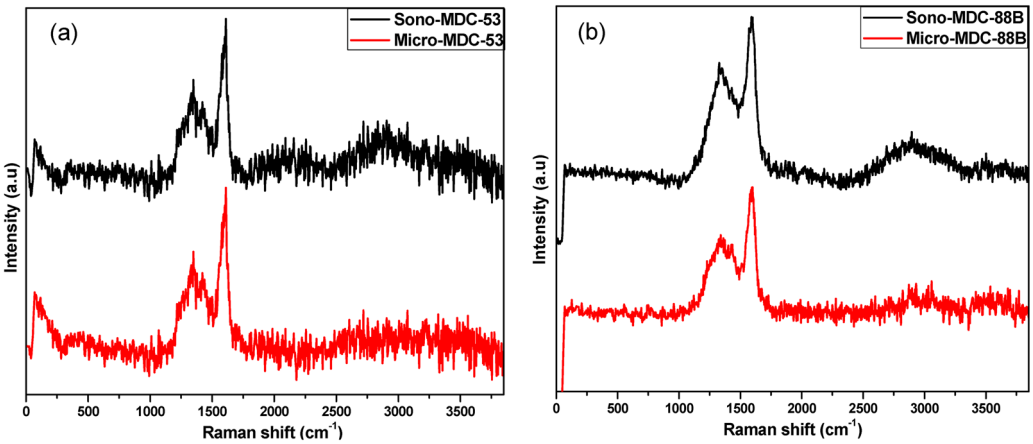


Fig. 5 Raman spectra of (a) MDC-53 and (b) MDC-88B samples.

Table 1 Raman analysis data

| Sample name | D band | G band | Intensity ratio ($A_D/A_G$) |
|---|---|---|---|
| Micro-MDC-53 | 1357 | 1610 | 1.29 |
| Sono-MDC-53 | 1348 | 1610 | 1.52 |
| Micro-MDC-88B | 1353 | 1602 | 1.67 |
| Sono-MDC-88B | 1357 | 1606 | 1.56 |

Type I and IV isotherm features corresponding to the hierarchical nature of the MOF materials (micropores and mesopores). The clear hysteresis loop in the isotherms is indicative of a mesoporous structure and arises from capillary condensation within mesopores. The surface areas of the prepared materials were below 35 $m^2\ g^{-1}$ and micropore volumes far below 0.1 $cm^3\ g^{-1}$ were obtained (Table 2). The low surface areas and pore volumes of the material might be due to the narrow pore configuration and/or the existence of trapped molecules within the pores of the sample. The results agree with previously obtained values.[23,48,49] Typical $N_2$ sorption isotherms of the MIL-88B MOF are shown in Fig. 6b. The isotherms of the

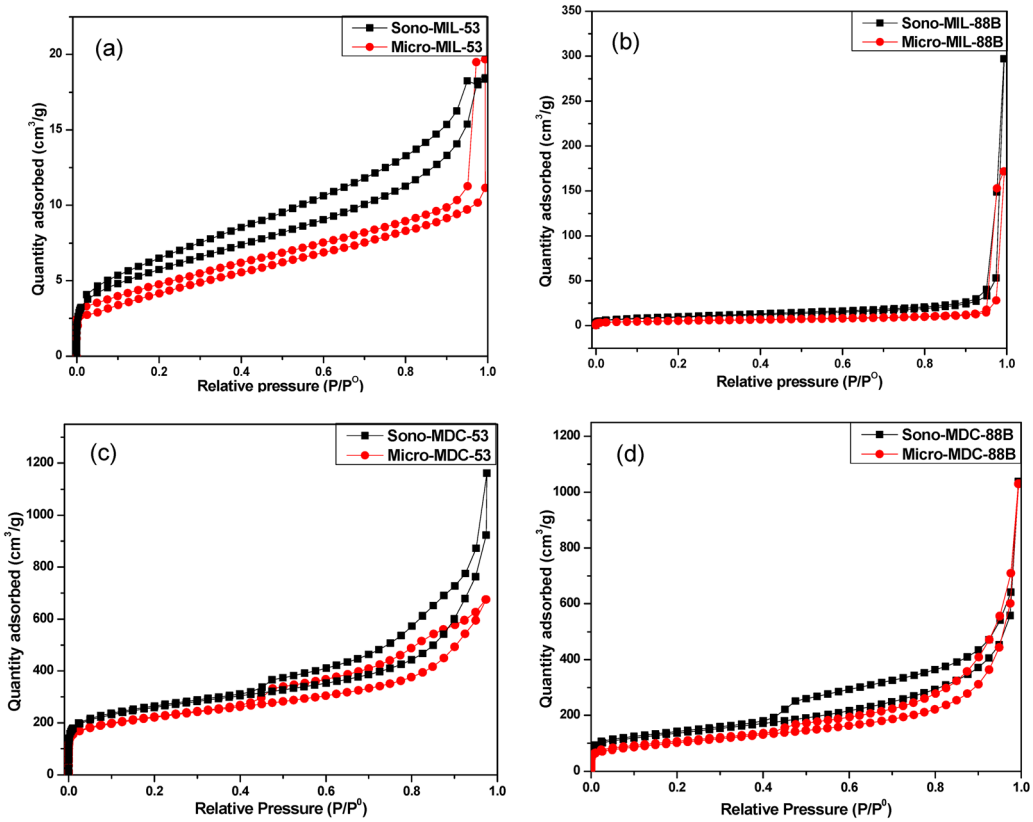


Fig. 6 $N_2$ adsorption–desorption isotherms of (a) Fe-MIL-53, (b) Fe-MIL-88B, (c) MDC-53 and (d) MDC-88B.

Open Access Article. Published on 12 november 2025. Downloaded on 11-05-2026 16:36:12.
This article is licensed under a Creative Commons Attribution 3.0 Unported Licence.

Table 2 Textural properties of Fe-MOFs and MDCs

| Sample name | BET ($m^2\ g^{-1}$) | Average micropore size (nm) | Pore volume ($cm^3\ g^{-1}$) | Micropore volume ($cm^3\ g^{-1}$) | $H_2$ uptake at 1 bar (wt%) | $CO_2$ uptake at 1 bar (mmol $g^{-1}$) |
|---|---|---|---|---|---|---|
| Micro-MIL-53 | 16 | 0.41 | 0.03 | 0.001 | | |
| Sono-MIL-53 | 20 | 0.70 | 0.54 | 0.008 | | |
| Micro-MIL-88B | 19 | 0.79 | 0.12 | 0.007 | | |
| Sono-MIL-88B | 34 | 0.66 | 0.13 | 0.013 | | |
| Micro-MDC-53 | 784 | 0.26 | 0.98 | 0.32 | 1.32 | 1.59 |
| Sono-MDC-53 | 947 | 0.35 | 1.44 | 0.38 | 1.20 | 2.09 |
| Micro-MDC-88B | 627 | 1.19 | 0.99 | 0.35 | 1.14 | 1.57 |
| Sono-MDC-88B | 650 | 1.75 | 0.85 | 0.43 | 1.17 | 1.47 |
| MOF-5-MDC[52] | 1884 | — | 1.84 | 0.59 | — | 2.43 |
| ZIF-8-MDC[53] | 716 | — | — | 0.25 | — | 2.66 |
| MOF-5-MDC[54] | 2393 | — | 1.13 | 0.34 | 2.7 | — |
| MIL-MDC-800[54] | 628 | — | 0.54 | 0.11 | 0.8 | — |
| C-1000[55] | 2872 | — | 2.06 | — | 2.60 | — |
| IRMOF-MDC-3[56] | 1678 | — | 2.01 | 0.66 | 2.1 | — |
| ZIF-8-C800[57] | 2169 | — | 1.50 | — | 2.23 | — |
| SFZ8C-700[58] | 1583 | — | — | — | — | 2.57 |
| C-800[59] | 464 | 3 | 0.25 | 0.11 | — | 1.36 |

prepared MOFs display distinctive attributes of an IUPAC Type I isotherm. The existence of micropores is indicated by the rapid uptake at low relative pressure ($p/p^0 < 0.05$). The microwave and sonochemically prepared samples had surface areas of 34 and 19 $m^2\ g^{-1}$, respectively.

$N_2$ adsorption–desorption isotherms of the derived carbons displayed hybrid IUPAC type I/IV isotherm features (Fig. 6c and d). The high $N_2$ uptake at low partial pressure is an indication of abundance of micropores. The H3 hysteresis loop at partial pressures above 0.4 signifies the existence of mesopores. The hysteresis loop of an H3-type commonly observed in carbon-based materials suggests the existence of slit-shaped pores. The surface areas of the MDCs drastically improved from 16–20 $m^2\ g^{-1}$ for the MIL-53 to 784–947 $m^2\ g^{-1}$ for the associated MDCs.

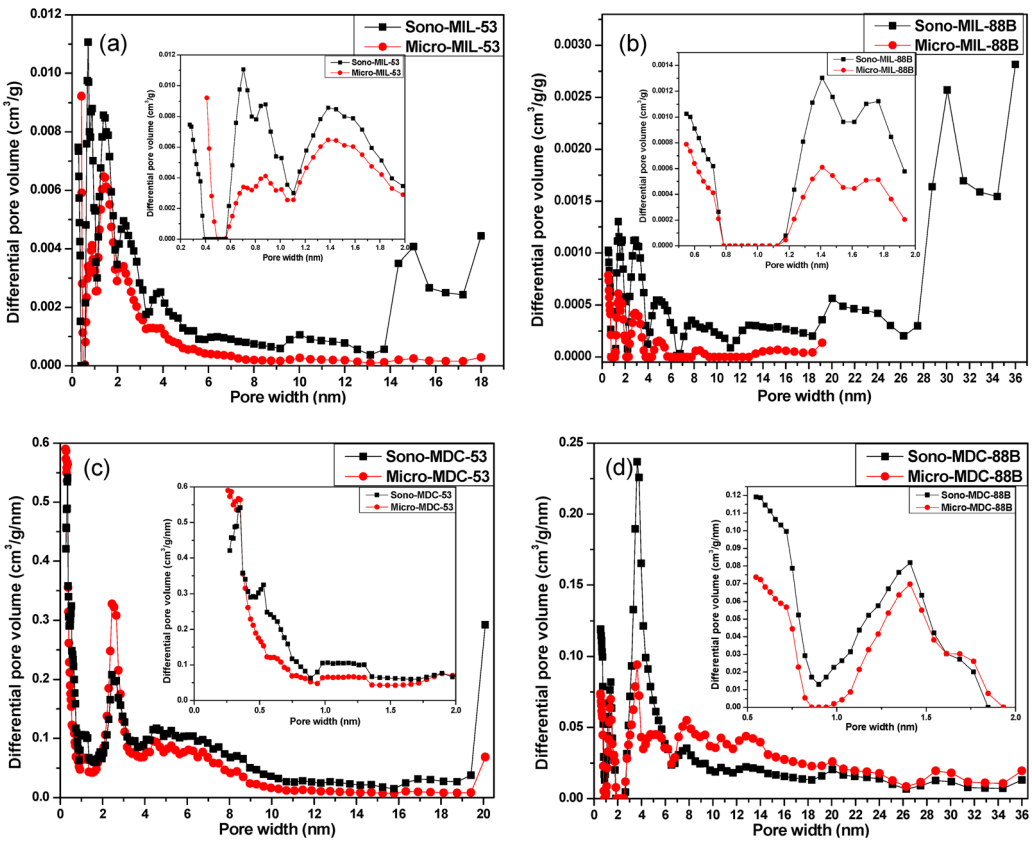


Fig. 7 Pore size distribution curves for (a) Fe-MIL-53, (b) Fe-MIL-88B, (c) MDC-53 and (d) MDC-88B. The insets are the pore size distribution curves in the microporous range.


© 2025 The Author(s). Published by the Royal Society of Chemistry

Open Access Article. Published on 12 november 2025. Downloaded on 11-05-2026 16:36:12.
This article is licensed under a Creative Commons Attribution 3.0 Unported Licence.

MIL-88B samples also displayed a major improvement from 19–34 $m^2 g^{-1}$ to 627–650 $m^2 g^{-1}$ for the corresponding MDCs. This improvement could be attributed to permanent porosity derived from direct carbonization.[28] Several reports have reported similar trends due to direct carbonization.[50,51]

The pore dimension distribution curves for both MIL-53 and MIL-88B (Fig. 7a and b) showed that the materials possess hierarchical pores (*i.e.* micropores and mesopores). The obtained results are aligned with those described in previous studies.[28,29] Similar to the parent MOF, hierarchical pore structures are evident for the MDCs but with superior differential pore volumes as revealed by their pore size distribution curves (Fig. 7c and d).

### 3.7. Hydrogen and carbon dioxide adsorption

Taking advantage of the superior textural properties of the MDCs, their $H_2$ and $CO_2$ uptakes were evaluated. Fig. 8a presents $H_2$ adsorption–desorption isotherms of the prepared carbons at 77 K, while Fig. 8b shows $CO_2$ adsorption–desorption isotherms at 298 K. The absence of a plateau in the adsorption isotherms, especially in $CO_2$ adsorption isotherms, indicates that the prepared materials still possess unsaturated adsorption sites at low pressures, implying a capacity for significantly enhanced uptakes under elevated pressures. The hierarchical pores of carbons are advantageous for fast gas transport, owing to the fact that mesopores act as low-resistance conduits that facilitate rapid diffusion toward micropores.[60] The hydrogen uptake was reasonable for the available surface areas. MIL-53 derived carbons displayed higher adsorption of hydrogen, with the highest uptake being 1.32 wt%, while the highest uptake for MIL-88B derived carbons is 1.17 wt%. The Sono-MDC-53 sample exhibited highest $CO_2$ uptake (2.09 mmol $g^{-1}$) due to the high availability of pores. MIL-88B derived carbons displayed relatively low gas uptakes, with the highest $CO_2$ uptake being 1.57 mmol $g^{-1}$ for Micro-MDC-88B (Table 2). After adsorption of the gases, desorption was performed and complete reversibility was achieved in all cases in line with a physisorption process (Fig. 8).

Other studies have previously reported adsorption capacities for MDCs at 1 bar and 77 K and 298 K for $H_2$ and $CO_2$, respectively (Table 2).[52–59] The porous carbons in those studies were derived from different types of MOFs (MOF-5, ZIF-8, IRMOF-3 and MIL-101) with much higher surface areas than the MIL-53 and MIL-88B MOFs synthesized in this study. Consequently, the derived carbons generally exhibited larger surface areas and pore volumes and therefore higher $H_2$ and $CO_2$ uptake than the MDCs in this study. MDCs derived from ZIF-8 are nitrogen-functionalized active microporous carbon and the pyrrolic–N present also contributed to the enhanced

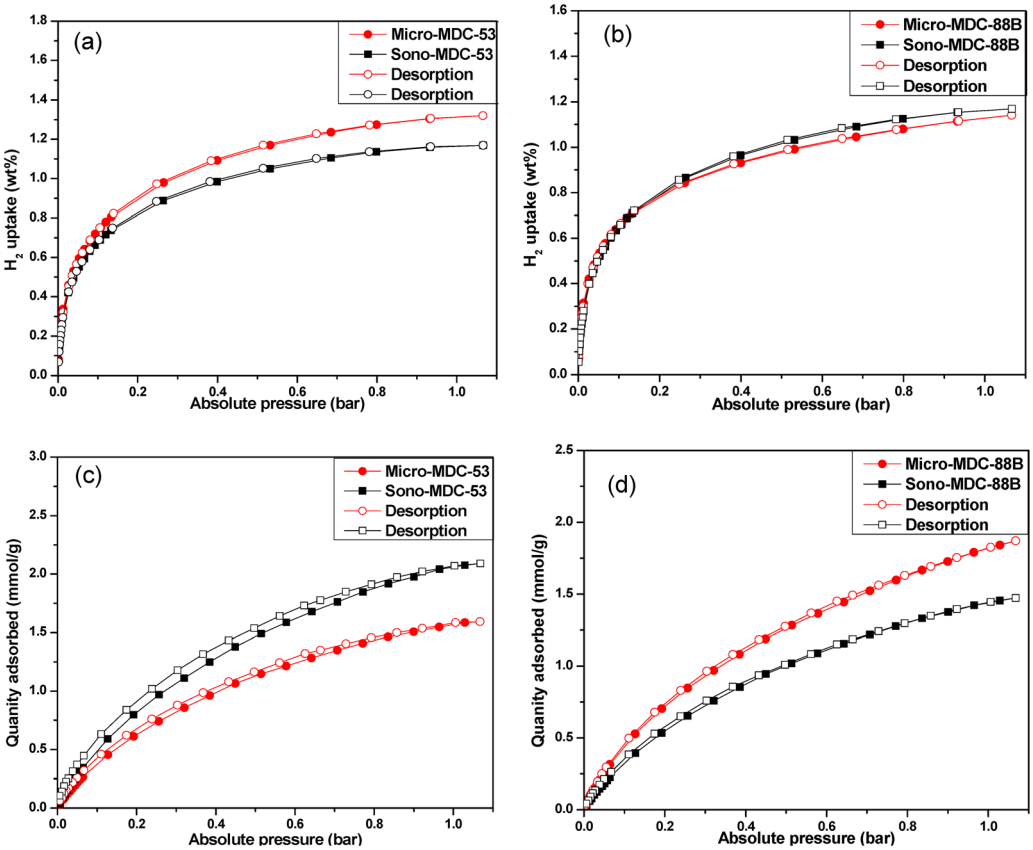


Fig. 8 (a) and (b) Hydrogen and (c) and (d) carbon dioxide uptake of the prepared MDCs at 77 K and 298K, respectively. Desorption data are represented with open symbols.

Open Access Article. Published on 12 november 2025. Downloaded on 11-05-2026 16:36:12.
This article is licensed under a Creative Commons Attribution 3.0 Unported Licence.

$CO_2$ uptake for ZIF-8-MDC.[53] It is also worth noting that unlike the MOFs used to prepare the MDCs from the literature reported in Table 2, the MOFs in the current study were synthesized *via* unconventional approaches and using waste precursors.

## 4. Conclusions

This study utilized waste-derived precursors to synthesize pure-phase Fe-based MOFs exhibiting a well-defined hexagonal bipyramidal morphology. Unconventional synthesis routes (*i.e.* sonochemical-assisted and microwave-assisted) were employed for the preparation of the Fe-MOFs, specifically MIL-53 and MIL-88B. The resulting materials exhibited moderate textural properties, characterized by relatively low surface areas and pore volumes, which were attributed to the inherent structural flexibility of these MOFs. The frameworks principally adopted narrow-pore or guest-loaded forms, which inherently limited accessible porosity.

Comprehensive characterization confirmed that the porosity and surface area of these flexible MOFs can be effectively enhanced *via* a direct carbonization approach. The process, conducted at a relatively low temperature (600 °C), yielded turbostratic carbon materials with a limited degree of graphitization and controlled defect density. This strategy markedly enhanced both the porosity and the surface area, with the highest recorded value of the surface area being 947 $m^2\ g^{-1}$. The resulting porous carbons also demonstrated appreciable $H_2$ and $CO_2$ adsorption capacities. The highest $H_2$ uptake was achieved at 1.32 wt% and the maximum $CO_2$ uptake was achieved at 2.09 mmol $g^{-1}$. Future work will include cyclic adsorption–desorption studies to assess the long-term $H_2$ and $CO_2$ storage performance of these porous carbon materials.

## Author contributions

Keaoleboga Mosupi: investigation, methodology, validation, formal analysis, and visualization, writing – original draft. Nqobile T Mthembu: investigation and writing – review and editing. Mike Masukume: resources and writing – review and editing. Nicholas M. Musyoka: conceptualization, methodology, supervision, funding acquisition, and writing – review and editing. Henrietta W. Langmi: conceptualization, supervision, funding acquisition, methodology, project administration, resources, and writing – review and editing.

## Conflicts of interest

There are no conflicts to declare.

## Data availability

The data that support the findings of this study will be available on reasonable request.

## Acknowledgements

MM and HWL acknowledge funding provided by the MAST3R-Boost project funded by the European Union (Call HORIZON-CL4-2021-RESILIENCE-01, grant agreement no. 101058574). HWL acknowledges the South African Research Chairs Initiative (SARChI) of the Department of Science, Technology and Innovation and the National Research Foundation (grant no. 2090155358), and NRF CPRR funding stream (grant no. 0215586378). NMM also acknowledges financial support provided by the Ningbo Yongjiang Talent Introduction Program (grant no. 2024A-176-G).

## References

1 J. L. Rowsell and O. M. Yaghi, Metal–organic frameworks: a new class of porous materials, *Microporous Mesoporous Mater.*, 2004, **73**(1–2), 3–14.
2 W. L. Teo, W. Zhou, C. Qian and Y. Zhao, Industrializing metal–organic frameworks: Scalable synthetic means and their transformation into functional materials, *Mater. Today*, 2021, **47**, 170–186.
3 Z. Xie and J. Hou, Industrialising Metal–Organic Frameworks—Bridging Laboratory Innovation and Future Applications, *Ind. Eng. Chem. Res.*, 2025, **64**(16), 7941–7955.
4 X. Dyosiba, J. Ren, N. M. Musyoka, H. W. Langmi, M. Mathe and M. S. Onyango, Preparation of value-added metal-organic frameworks (MOFs) using waste PET bottles as source of acid linker, *Sustainable Mater. Technol.*, 2016, **10**, 10–13.
5 Y. He, Y. Luo, M. Yang, Y. Zhang, L. Zhu, M. Fan and Q. Li, Selective catalytic synthesis of bio-based terephthalic acid from lignocellulose biomass, *Appl. Catal., A*, 2022, **630**, 118440.
6 Y. Tachibana, S. Kimura and K.-I. Kasuya, Synthesis and verification of biobased terephthalic acid from furfural, *Sci. Rep.*, 2015, **5**(1), 8249.
7 S. Wang and X. Wang, Synergistic flame retardancy of MIL-88B-Fe metal–organic framework with aluminum diethyl hypophosphite in epoxy resin, *J. Vinyl Addit. Technol.*, 2025, **31**(4), 824–838.
8 J. M. Gonçalves, J. V. Brandao and B. S. Neto, A synthesis of metal–organic frameworks using terephthalic acid obtained from PET bottles with dye adsorption for application in experimental chemistry classes, *Discover Chem.*, 2025, **2**(1), 144.
9 J. Na, K. Pandi, G. Nam and J. Jung, Upcycling of plastic wastes, polyethylene terephthalate (PET) into photocatalyst under visible light: Application for dye removal, *J. Ind. Eng. Chem.*, 2025, **148**, 483–491.
10 S. Cheng, Y. Li, Z. Yu, R. Gu, W. Wu and Y. Su, Waste PET-derived MOF-5 for high-efficiency removal of tetracycline, *Sep. Purif. Technol.*, 2024, **339**, 126490.
11 K.-W. Jung, J.-H. Kim and J.-W. Choi, Synthesis of magnetic porous carbon composite derived from metal-organic framework using recovered terephthalic acid from polyethylene


© 2025 The Author(s). Published by the Royal Society of Chemistry

Open Access Article. Published on 12 november 2025. Downloaded on 11-05-2026 16:36:12.
This article is licensed under a Creative Commons Attribution 3.0 Unported Licence.

terephthalate (PET) waste bottles as organic ligand and its potential as adsorbent for antibiotic tetracycline hydrochloride, *Composites, Part B*, 2020, **187**, 107867.

12 K. Mosupi, M. Masukume, G. Weng, N. M. Musyoka and H. W. Langmi, Recent advances in Fe-based metal-organic frameworks: Structural features, synthetic strategies and applications, *Coord. Chem. Rev.*, 2025, **529**, 216467.

13 J. Chen, K. Shen and Y. Li, Greening the processes of metal–organic framework synthesis and their use in sustainable catalysis, *ChemSusChem*, 2017, **10**(16), 3165–3187.

14 P. Horcajada, F. Salles, S. Wuttke, T. Devic, D. Heurtaux, G. Maurin, A. Vimont, M. Daturi, O. David and E. Magnier, How linker's modification controls swelling properties of highly flexible iron(III) dicarboxylates MIL-88, *J. Am. Chem. Soc.*, 2011, **133**(44), 17839–17847.

15 C. Mellot-Draznieks, C. Serre, S. Surblé, N. Audebrand and G. Férey, Very large swelling in hybrid frameworks: a combined computational and powder diffraction study, *J. Am. Chem. Soc.*, 2005, **127**(46), 16273–16278.

16 M. Guo and H. Li, The Hydrolyzed Mil-88B (Fe) With improved surface area for high-capacity lithium ion battery, *Front. Energy Res.*, 2021, **9**, 781008.

17 F. Millange, N. Guillou, R. I. Walton, J.-M. Grenèche, I. Margiolaki and G. Férey, Effect of the nature of the metal on the breathing steps in MOFs with dynamic frameworks, *Chem. Commun.*, 2008, 4732–4734.

18 P. Horcajada, C. Serre, G. Maurin, N. A. Ramsahye, F. Balas, M. Vallet-Regí, M. Sebban, F. Taulelle and G. Férey, Flexible porous metal-organic frameworks for a controlled drug delivery, *J. Am. Chem. Soc.*, 2008, **130**(21), 6774–6780.

19 N. Aljammal, C. Jabbour, S. Chaemchuen, T. Juzsakova and F. Verpoort, Flexibility in metal–organic frameworks: A basic understanding, *Catalysts*, 2019, **9**(6), 512.

20 H. J. Lee, W. Cho, E. Lim and M. Oh, One-pot synthesis of magnetic particle-embedded porous carbon composites from metal–organic frameworks and their sorption properties, *Chem. Commun.*, 2014, **50**(41), 5476–5479.

21 N. T. Mthembu, Holistic synthesis of iron-based metal–organic frameworks using unconventional metal feedstock and polyethylene terephthalate derived organic linkers, MSc Thesis, University of Pretoria, South Africa, 2022.

22 R. El Osta, A. Carlin-Sinclair, N. Guillou, R. I. Walton, F. Vermoortele, M. Maes, D. de Vos and F. Millange, Liquid-phase adsorption and separation of xylene isomers by the flexible porous metal–organic framework MIL-53 (Fe), *Chem. Mater.*, 2012, **24**(14), 2781–2791.

23 E. Yılmaz, E. Sert and F. S. Atalay, Synthesis, characterization of a metal organic framework: MIL-53 (Fe) and adsorption mechanisms of methyl red onto MIL-53 (Fe), *J. Taiwan Inst. Chem. Eng.*, 2016, **65**, 323–330.

24 Z. Qin, M. Sun, R. Wu, P. Li, R. Tai, H. Su, J. Tressel, B. Ji, Q. Wang and S. Chen, Photocatalytic Degradation of Organic Pollutants by Sulfate Radicals Activated by Defective NH2-MIL-88B, *Langmuir*, 2025, **41**(19), 12311–12323.

25 Z. Qin, R. Wu, S. Gao, R. Tai, P. Li, X. Sui, X. Song, Q. Wang and S. Chen, Photocatalytic degradation of pollutants by self-Fenton reaction on defective NH2-MIL-88B with on-site production of hydrogen peroxide, *Appl. Surf. Sci.*, 2025, **695**, 162870.

26 N. P. Makhanya, B. Oboirien, N. Musyoka, J. Ren and P. Ndungu, Evaluation of PET-derived metal organic frameworks (MOFs) for water adsorption and heat storage, *J. Porous Mater.*, 2023, **30**(2), 387–401.

27 L. T. Tran, H. T. Dang, H. V. Tran, G. T. Hoang and C. D. Huynh, MIL-88B (Fe)-NH 2: An amine-functionalized metal–organic framework for application in a sensitive electrochemical sensor for Cd 2+, Pb 2+, and Cu 2+ ion detection, *RSC Adv.*, 2023, **13**(32), 21861–21872.

28 T. Van Tran, D. T. C. Nguyen, H. T. Le, T. T. Tu, N. D. Le, K. T. Lim, L. G. Bach and T. D. Nguyen, MIL-53 (Fe)-directed synthesis of hierarchically mesoporous carbon and its utilization for ciprofloxacin antibiotic remediation, *J. Environ. Chem. Eng.*, 2019, **7**(1), 102881.

29 T. Van Tran, V. Dai Cao, V. H. Nguyen, B. N. Hoang, D.-V. N. Vo, T. D. Nguyen and L. G. Bach, MIL-53 (Fe) derived magnetic porous carbon as a robust adsorbent for the removal of phenolic compounds under the optimized conditions, *J. Environ. Chem. Eng.*, 2020, **8**(1), 102902.

30 R. Sun, H.-B. Zhang, J. Yao, D. Yang, Y.-W. Mai and Z.-Z. Yu, In situ reduction of iron oxide with graphene for convenient synthesis of various graphene hybrids, *Carbon*, 2016, **107**, 138–145.

31 M. Wang, X. Zhang, L. Zhou and Y. Chen, Activated MIL-53 (Al) for efficient adsorption of dichloromethane and trichlormethane, *Aerosol Air Qual. Res.*, 2016, **16**(8), 2003–2010.

32 T. Ahnfeldt, D. Gunzelmann, T. Loiseau and D. Hirsemann, Senker, J. r.; Férey, G.; Stock, N., Synthesis and modification of a functionalized 3D open-framework structure with MIL-53 topology, *Inorg. Chem.*, 2009, **48**(7), 3057–3064.

33 A. Boutin, D. Bousquet, A. U. Ortiz, F.-X. Coudert, A. H. Fuchs, A. Ballandras, G. Weber, I. Bezverkhyy, J.-P. Bellat and G. Ortiz, Temperature-induced structural transitions in the gallium-based MIL-53 metal–organic framework, *J. Phys. Chem. C*, 2013, **117**(16), 8180–8188.

34 Z.-F. Yu, Y. Yang, H.-F. Zhuang, S.-D. Shan, M.-S. Beldean-Galea, Q.-Q. Xue, X.-F. Shen and S.-J. Li, In-situ growth of MIL-53 (Fe) on charcoal sponge as a highly efficient and recyclable photocatalyst for removal of Cr (VI), *Rare Met.*, 2024, **43**(9), 4344–4355.

35 T. T. Quang, N. X. Truong, T. H. Minh, N. N. Tue and G. T. P. Ly, Enhanced photocatalytic degradation of MB under visible light using the modified MIL-53 (Fe), *Top. Catal.*, 2020, **63**(11), 1227–1239.

36 X. Guo and D. Yin, Fabrication of a novel hybrid MIL-53 (Fe)/MoSe2 with outstanding photocatalytic performances, *Ionics*, 2022, **28**(8), 3907–3917.

37 X. Yi, X. He, F. Yin, T. Yang, B. Chen and G. Li, NH 2–MIL-88B–Fe for electrocatalytic N 2 fixation to NH 3 with high faradaic efficiency under ambient conditions in neutral electrolyte, *J. Mater. Sci.*, 2020, **55**, 12041–12052.

38 M. Ma, A. Bétard, I. Weber, N. S. Al-Hokbany, R. A. Fischer and N. Metzler-Nolte, Iron-based metal–organic frameworks

Open Access Article. Published on 12 november 2025. Downloaded on 11-05-2026 16:36:12.
This article is licensed under a Creative Commons Attribution 3.0 Unported Licence.

MIL-88B and NH2-MIL-88B: high quality microwave synthesis and solvent-induced lattice ''breathing'', *Cryst. Growth Des.*, 2013, **13**(6), 2286–2291.

39 L. W. Aguiar, G. P. Otto, V. L. Kupfer, S. L. Fávaro, C. T. P. Silva, M. P. Moisés, L. de Almeida, M. R. Guilherme, E. Radovanovic and E. M. Girotto, Simple, fast, and low-cost synthesis of MIL-100 and MIL-88B in a modified domestic microwave oven, *Mater. Lett.*, 2020, **276**, 128127.

40 R. Lin, S. Li, J. Wang, J. Xu, C. Xu, J. Wang, C. Li and Z. Li, Facile generation of carbon quantum dots in MIL-53 (Fe) particles as localized electron acceptors for enhancing their photocatalytic Cr (vi) reduction, *Inorg. Chem. Front.*, 2018, **5**(12), 3170–3177.

41 F. Qi, L. He, L. Cui, W. Wang, K. H. Siddique and S. Li, Smart antibacterial food packaging based on MIL-53 (Fe) functionalized polylactic acid film for pH-responsive controlled release, *J. Polym. Environ.*, 2023, **31**(9), 4022–4032.

42 A. Nikseresht, R. Bagherinia, M. Mohammadi and R. Mehravar, Phosphomolybdic acid hydrate encapsulated in MIL-53 (Fe): a novel heterogeneous heteropoly acid catalyst for ultrasound-assisted regioselective nitration of phenols, *RSC Adv.*, 2023, **13**(1), 674–687.

43 M. E. Elmowafy, O. Abuzalat, A. Baraka, M. A. Elsayed, M. F. Hagag, R. Sadek and H. Tantawy, Exploring a novel approach for the synthesis of MIL-53 (Fe)/reduced graphene oxide composites with preserved structural integrity for high performance for electromagnetic wave shielding, *Discover Appl. Sci.*, 2024, **6**(4), 161.

44 A. Golmohamadpour, B. Bahramian, A. Shafiee and L. Ma'mani, Slow released delivery of alendronate using β-cyclodextrine modified Fe-MOF encapsulated porous hydroxyapatite, *J. Inorg. Organomet. Polym. Mater.*, 2018, **28**, 1991–2000.

45 Y. T. Gong, B. H. Li, T. Pei, C. H. Lin and S. Lee, Raman investigation on carbonization process of metal–organic frameworks, *J. Raman Spectrosc.*, 2016, **47**(10), 1271–1275.

46 E. Dervishi, Z. Ji, H. Htoon, M. Sykora and S. K. Doorn, Raman spectroscopy of bottom-up synthesized graphene quantum dots: size and structure dependence, *Nanoscale*, 2019, **11**(35), 16571–16581.

47 L. S. Blankenship, N. Balahmar and R. Mokaya, Oxygen-rich microporous carbons with exceptional hydrogen storage capacity, *Nat. Commun.*, 2017, **8**(1), 1–12.

48 J. Gordon, H. Kazemian and S. Rohani, MIL-53 (Fe), MIL-101, and SBA-15 porous materials: potential platforms for drug delivery, *Mater. Sci. Eng., C*, 2015, **47**, 172–179.

49 T. A. Vu, G. H. Le, C. D. Dao, L. Q. Dang, K. T. Nguyen, Q. K. Nguyen, P. T. Dang, H. T. Tran, Q. T. Duong and T. V. Nguyen, Arsenic removal from aqueous solutions by adsorption using novel MIL-53 (Fe) as a highly efficient adsorbent, *RSC Adv.*, 2015, **5**(7), 5261–5268.

50 M. Ding, W. Shi, L. Guo, Z. Y. Leong, A. Baji and H. Y. Yang, Bimetallic metal–organic framework derived porous carbon nanostructures for high performance membrane capacitive desalination, *J. Mater. Chem. A*, 2017, **5**(13), 6113–6121.

51 X.-M. Cao, Z.-J. Sun, S.-Y. Zhao, B. Wang and Z.-B. Han, MOF-derived sponge-like hierarchical porous carbon for flexible all-solid-state supercapacitors, *Mater. Chem. Front.*, 2018, **2**(9), 1692–1699.

52 W. Kukulka, K. Cendrowski, B. Michalkiewicz and E. Mijowska, MOF-5 derived carbon as material for CO 2 absorption, *RSC Adv.*, 2019, **9**(32), 18527–18537.

53 S. Gadipelli and Z. X. Guo, Tuning of ZIF-derived carbon with high activity, nitrogen functionality, and yield–a case for superior CO2 capture, *ChemSusChem*, 2015, **8**(12), 2123–2132.

54 T. Segakweng, N. M. Musyoka, J. Ren, P. Crouse and H. W. Langmi, Comparison of MOF-5-and Cr-MOF-derived carbons for hydrogen storage application, *Res. Chem. Intermed.*, 2016, **42**(5), 4951–4961.

55 B. Liu, H. Shioyama, T. Akita and Q. Xu, Metal-organic framework as a template for porous carbon synthesis, *J. Am. Chem. Soc.*, 2008, **130**(16), 5390–5391.

56 S. J. Yang, T. Kim, J. H. Im, Y. S. Kim, K. Lee, H. Jung and C. R. Park, MOF-derived hierarchically porous carbon with exceptional porosity and hydrogen storage capacity, *Chem. Mater.*, 2012, **24**(3), 464–470.

57 H.-L. Jiang, B. Liu, Y.-Q. Lan, K. Kuratani, T. Akita, H. Shioyama, F. Zong and Q. Xu, From metal–organic framework to nanoporous carbon: toward a very high surface area and hydrogen uptake, *J. Am. Chem. Soc.*, 2011, **133**(31), 11854–11857.

58 Y. Xiao, H. Yang, X. Bu and P. Feng, ZIF-8 derived carbon materials with multifunctional selective adsorption abilities, *Carbon*, 2021, **176**, 421–430.

59 W. Wang and D. Yuan, Mesoporous carbon originated from non-permanent porous MOFs for gas storage and $CO_2/CH_4$ separation, *Sci. Rep.*, 2014, **4**(1), 5711.

60 X. Ma, L. Li, R. Chen, C. Wang, H. Li and S. Wang, Heteroatom-doped nanoporous carbon derived from MOF-5 for CO2 capture, *Appl. Surf. Sci.*, 2018, **435**, 494–502.


© 2025 The Author(s). Published by the Royal Society of Chemistry